Electrochemical Sensing of Luteolin from Straw Pyrolysis Carbon Prepared by Molten Salt Carbonization

[1, 2] Youluan Lu, [1, 2] Xinwei Mu, [1, 2] Yaopeng Liu, [2] Zhen Shi, [1, 2] Yin Zheng*
[2] Wensheng Huang, and [2] Fangming Lou
[1]Hubei Key Laboratory of Biologic Resources Protection and Utilization,
Hubei Minzu University, Enshi 445000, China.
[2]School of Chemical and Environmental Engineering, Hubei Minzu University, Enshi 445000, China.
zhengyin0617@163.com*

Summary: In order to well use waste biomass and realise the quantitative analysis of luteolin, the sorghum straw from the old broom was used to prepare biomass carbon material (CMS-PCSS) through the molten salt carbonization. Then the CMS-PCSS was characterised by scanning electron microscopy (SEM), transmission electron microscopy (TEM), X-ray diffraction (XRD), X-ray photoelectron spectroscopy (XPS) Raman spectra (Raman), and N_2 sorption analysis. In addition, the electrochemical performance of the CMS-PCSS based sensors was examined by electrochemical impedance spectroscopy (EIS) and cyclic voltammetry (CV). Under the first-rank experimental conditions, the electrochemical sensor established with this material performed well in the quantitative analysis and actual sample detection of luteolin, the detection range of luteolin was 0.05~10.0 μmol/L, and the actual achievable minimum detection limit was 0.019 μmol/L.

Keywords: Analytical chemistry, Electrochemical sensor, Biomass pyrolytic carbon, Molten salt carbonization, Luteolin.

Introduction

Luteolin (3′,4′,5,7-tetrahydroxyflavone) is a flavonoid present in a vast variety of plants, with various biomedical applications such as anticancer anti-inflammatory and antibacterial agent [1-3]. Moreover, luteolin also exhibits potential curative efficacy of cataract prevention in clinical application [4]. Based on these performances, luteolin is receiving more and more attention. Therefore, it is significant to establish an efficient and sensitive detection method for luteolin. The reported quantitative detection methods of luteolin, including capillary electrophoresis [5], thin-layer chromatography [6], spectrophotometry [7], and high-performance liquid chromatography [8], often need a complex pretreatment process, expensive instruments or long detection time. In comparison with the above mentioned methods, the electrochemical sensing can overcome these shortcomings [9-11], so it is more suitable for detecting the content of luteolin than other methods. However, the response of the glassy carbon electrode (GCE) to rutin was limited, the most direct and effective scheme to find suitable modification materials to modify the electrode.

The reported modified materials for the construction of luteolin electrochemical sensors include graphene composites [4], carbon dots [12], and porous carbon doped with gold nanoparticles [13]. The preparation of these materials is cumbersome and costly. Compared to these materials, the biomass pyrolytic carbon not only has a low cost and simple preparation process, but also has rich pore structure, large specific surface area and good stability electrical conductivity, thus it is more suitable for electrode modification materials. Among many biomass raw materials, straw is a wide choice of source material. The carbon materials derived from straw have been used to construct electrochemical sensors. However, in these reports, the preparation process of straw pyrolytic carbon was complicated, a large amount of strong acid and strong base was needed in the preparation process, and nano-metal was doped due to the unsatisfactory electrochemical performance of the carbon materials [14, 15]. These schemes not only fail to give full play to the material properties of straw, but also hinder the large-scale preparation and application of straw pyrolytic carbon. Therefore, it is necessary to explore new preparation methods of straw pyrolytic carbon to solve these problems. The molten salt carbonization method, not only gives the biomass pyrolytic carbon material developed pore structure and specific surface area, but also has the advantages of mild reaction environment, simple operation method and low requirements on equipment performance [16, 17], thus it aroused the author's interest. Due to the unique carbonization effect in the molten state, the NaCl has been applied in the preparation of biomass by molten salt carbonization [18, 19].

---

*To whom all correspondence should be addressed.

In this work, the sorghum straw was employed from the old broom as the precursor, then it was mixed with NaCl to prepare biomass pyrolytic carbon (CMS-PCSS) by the one-step pyrolysis method. Based on CMS-PCSS, an electrochemical sensor was constructed, and the electrochemical behaviour and possible reaction mechanism of luteolin on the sensor were studied. The method proposed in this work not only has a low detection limit but also performs well in real sample analysis.

Experimental

Reagents and apparatus

Sorghum straw (SS) was taken from a discarded broom. NaCl, N,N-Dimethylformamide, chemically pure. Luteolin, analytical reagent. All drugs were purchased from Chinese Pharmaceutical Group Chemical Reagent Co., Ltd, China. The phosphoric acid, potassium dihydrogen phosphate and disodium hydrogen phosphate were used as supporting electrolytes (PBS) for the concentration of 0.1 mol/L.

Electrochemical tests were worked on the CHI660E electrochemical workstation (Shanghai Chenhua, China). The three-electrode electrochemical system consists of a GCE (3 mm diameter, working electrode), an Hg/HgCl (reference electrode) and a Pt wire (auxiliary). PHS-3C pH meter (Shanghai Leici Instrument Co. Ltd., Shanghai, China). P680LPG high performance liquid chromatographic (HPLC, Agilent, America). Quanta FEG 250 Scanning Electron Microscope (SEM, FEI, American). Tecnai G2 F20 transmission electron microscopy (TEM, FEI, American). X-ray diffraction (XRD, SHIMADZU, Japan). Thermo ESCALAB 250XI photoelectron spectroscopy (XPS, Thermo Scientific, America). N_2 sorption analysis was recorded on the QUADRASORB SI porosimeter (Quantachrome, America) and the pore size distribution plots were evaluated based on density functional theory (DFT). Thermo Fischer DXR Raman spectrometer (Raman, Thermo Scientific, America).

Synthesis of materials

The SS was chopped in fraction lets (about 0.5 cm^2 area), then washed with ultrapure water and dried at 90°C for 10 h in a vacuum loft drier to obtain the precursor. The obtained precursor was subsequently mixed with NaCl at a 1:1 volume ratio, then pyrolytic treated in N_2 atmosphere at 5°C/min and maintained for 2 h at 801°C. After high-temperature pyrolysis, the samples were washed with ultrapure water at 50°C and ultrasonic for 0.5 h to recycle NaCl, then washed 3 times with 0.5 mol/L HCl, ultrapure water, respectively. Finally, the products were filtered and dried to achieve pyrolytic carbon of sorghum stalks. As a comparison, the preparation method of the pyrolytic carbon from sorghum stalks (PCSS) was the same as the CMS-PCSS just without NaCl.

Fabrication of the modified electrode

Before each modification, the bare GCE was polished with 0.05 μm Al_2O_3 slurry firstly, then washed thoroughly with dilute HNO_3, ethanol, ultrapure water, respectively. The CMS-PCSS and the PCSS was dispersed into the DMF by ultrasonic for 3h to achieve a dispersion solution of 10 mg/mL concentration, respectively. Under the infrared lamp, 5.0 μL dispersion droplets were cast onto the pretreated GCE surface and dried. The obtained modified electrodes were labelled as CMS-PCSS/GCE and PCSS/GCE, respectively.

Electrochemical measurements

Electrochemical impedance spectroscopy (EIS) and cyclic voltammetry (CV) were carried out in an aqueous solution containing 0.1 mol/L KCl and 5 mmol/L $[Fe (CN)_6]^{3-/4-}$. The electrochemical performance of the samples was characterised by CV and differential pulse voltammetry (DPV) techniques, which supporting electrolyte were 0.1 mol/L PBS. All the work was implemented with a CHI660E electrochemical workstation at room temperature in a three-electrode system.

Summary of abbreviations

Table-1: Comparison table of abbreviations and full names in this paper.

The full name	Abbreviation
Sorghum straw	SS
Pyrolytic carbon of sorghum straw prepared by direct pyrolysis	PCSS
Pyrolytic carbon of sorghum straw prepared by molten salt carbonization	CMS-PCSS
N,N-Dimethylformamide	DMF
Phosphate buffer solution	PBS
Glassy carbon electrode	GCE
High performance liquid chromatographic	HPLC
Scanning Electron Microscope	SEM
Transmission electron microscopy	TEM
X-ray diffraction	XRD
X-ray photoelectron spectroscopy	XPS
Raman spectrometer	Raman
Electrochemical impedance spectroscopy	EIS
Cyclic voltammetry	CV
Differential pulse voltammetry	DPV

Results and Discussion

Characterisation of materials

SEM images (Fig.1) showed the surface morphology of the PCSS (a) and the CMS-PCSS (b). It looked like the pores on the surface of the CMS-PCSS were more evenly distributed than the PCSS. Fig. 1 (c) and (d) was the TEM image of the PCSS and the CMS-PCSS, respectively. It can be seen that the internal pore structure of CMS-PCSS was more developed, which may be due to under the N_2 atmosphere and high temperature, CO_2 and H_2O gases produced by biomass decomposition escape to form pore structure, while liquid molten salt will flow and fill the pores in the material and continue to react with the inorganic components in the material to derive more developed pore structure in the CMS-PCSS.
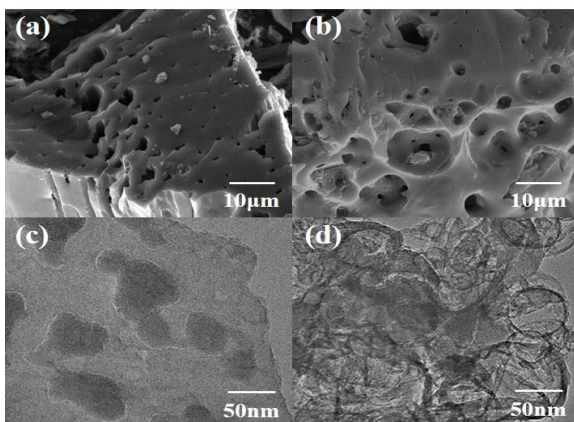

Fig. 1: (a), (b) is the SEM picture of the PCSS and the CMS-PCSS, and (c), (d) is the TEM picture of the PCSS and the CMS-PCSS, respectively.

Fig. 2 showed XRD patterns of the PCSS and the CMS-PCSS. It indicated that the graphitic stacking diffraction peaks of these materials were 22.2° and 43.5°, corresponding to 002 and 100 crystal planes, the diffraction peaks of CMS-PCSS at 43.5° was more sharp, reflected that the CMS-PCSS owned the higher degree of graphitization [20].

Furthermore, Raman spectra were also used to explore the structures of the materials (Fig.3). The strong characteristic peaks D (1350 cm^{-1}) and G (1590 cm^{-1}) correspond to the defects of graphite structure and the in-plane oscillation bands of the graphite layer, respectively. We can know that the I_D/I_G of the PCSS was 1.02 and the I_D/I_G of the CMS-PCSS was 0.95, which suggested that the CMS-PCSS

had a higher degree of graphitisation, which was consistent with the XRD analysis above [21].
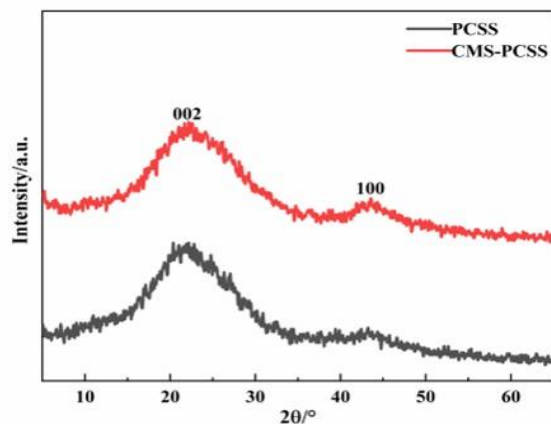

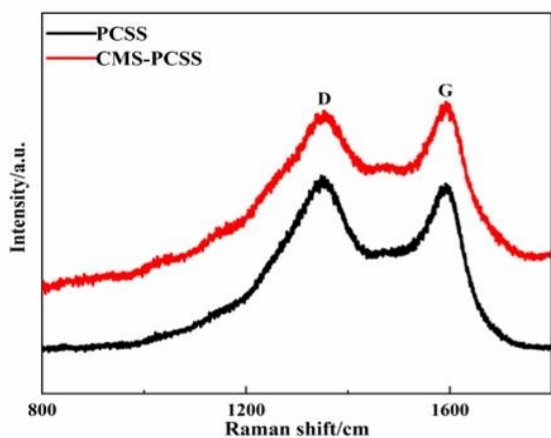
Fig. 2: XRD pattern of the PCSS and the CMS-PCSS.

Fig. 3: Raman spectra of the PCSS and the CMS-PCSS.

XPS was used to characterise the composition of the PCSS and the CMS-PCSS (Fig.4). As shown in Fig. 4(a), the binding energies of 284 and 531 eV were respective accredited to C1s and O1s. Compared with PCSS, the proportion of C increased and the O decreased in the CMS-PCSS. Peaks in Fig. 4(b) included C=C (283.5 eV), C=N (284 eV) and C=O (285 eV). Fig. 4(c) indicated the component of the O1s XPS spectrum, which peaks at 531.2 eV and 532.2 eV binding energies agreed to the O-C and O-C=O species, respectively. The existence of C=N could improve the active sites on the surface of carbon materials [22], and the abundant O content can improve the electrochemical performance of the material [23].
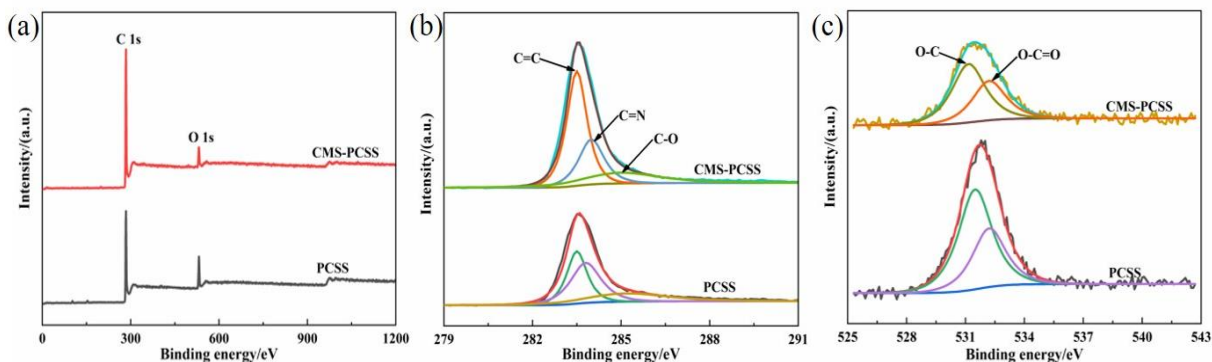
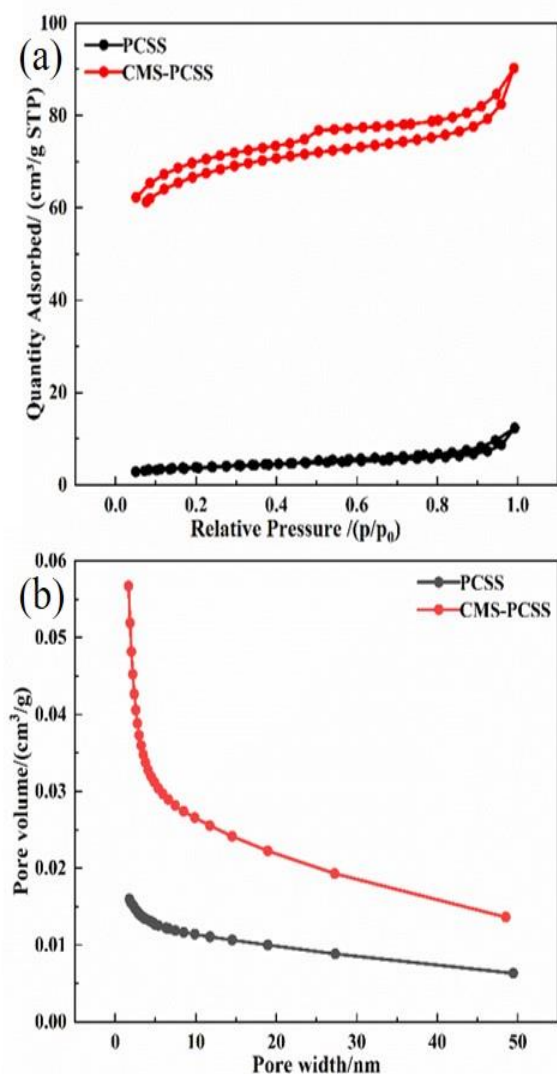Fig. 4: XPS spectra (a), C 1s(b), and O 1s(d) fitting of PCSS and CMS-PCSS.

Fig. 5: N$_2$ sorption isotherm (a) and pore size distribution curves (b) of PCSS and CMS-PCSS.

The specific surface area and pore size distributions have a great influence on the properties of carbon materials, so N$_2$ sorption analysis was applied to analyse these properties of the materials ulteriorly (Fig.5). Based on the Barrett-Joyner-Halenda (BJH) method, the specific surface area of PCSS and CMS-PCSS was 12.94 m^2/g and 415.1 m^2/g, and the pore volume of PCSS and CMS-PCSS was 0.0018 cm^3/g and 0.1782 cm^3/g, respectively. The reason for this result was that liquid molten salts reacted with inorganic components in the material to generate developed pore structures, which greatly increased the specific surface area and the pore volume of CMS-PCSS. Furthermore, as can be seen from Fig.5 (b), the microporous structure of CMS-PCSS was very well developed, this structure can effectively increase the absorption capacity of the measured substance on the sensor surface [24, 25].

Electrochemical investigations

The electrochemical characteristics of the GCE, PCSS/GCE and CMS-PCSS/GCE were investigated by CV and EIS in 5 mmol/L [Fe(CN)$_6$]$^{3-/4-}$ containing 0.1 mol/L KCl. Fig. 6(a) showed the Nyquist plots of different electrodes in the frequency range from 10^5 to 0.01 Hz. It turned out that the arc radius of the CMS-PCSS/GCE in the high-frequency region was smaller than other sensors, which indicated that the sensor surface had lower charge transfer resistance and a faster electron transport rate than other electrodes. As shown in Fig. 6(b), CMS-PCSS/GCE owned a larger electric capacity than other electrodes, it suggested that the sensor had the highest electroactivity. These results were attributed to the high degree of graphitization, developed specific surface area and microporous structure of CMS-PCSS.
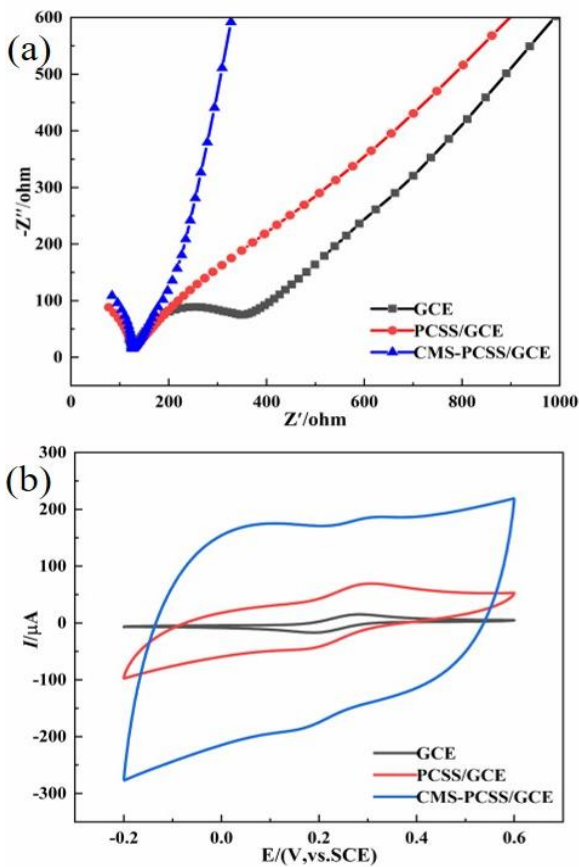
Fig. 7:   DPV curves of different sensors in PBS 3.0 containing 10 µmol/L luteolin.

Fig. 6:   EIS (a) and CV (b) curves of different electrodes in 5 mmol/L [Fe $(CN)_6]^{3-/4-}$ containing 0.1 mol/L KCl.

Fig.7 showed the DPV depictions of different electrodes in pH 3.0 PBS containing 10µmol/L luteolin. As shown in the diagram, the luteolin showed the strongest electrochemical response to the CMS-PCSS/GCE, which was attributed to the higher specific surface area and stronger conductivity of CMS-PCSS.

The effect of buffer pH on the electrochemical behaviour of luteolin on the CMS-PCSS/GCE was also investigated. As shown in Fig. 8(a), the response current decreased with the increase of pH. When the pH value of the electrolyte solution was 3.0, the largest current value appeared (Fig. 8(b)), so the pH 3.0 PBS was selected as the optimum buffer solution. Meanwhile, from Fig. 8(b) it can be known that the peak potentials (E) decreased linearly with the increase of pH and the fitting equation was E (V) = (0.685 ± 0.005) - (0.061 ± 0.001) pH, the slope value was very close to the Nernst slope, pointing that an equal number of H^+ and e^- were involved in the electrochemical reaction on the CMS-PCSS/GCE surface [26].
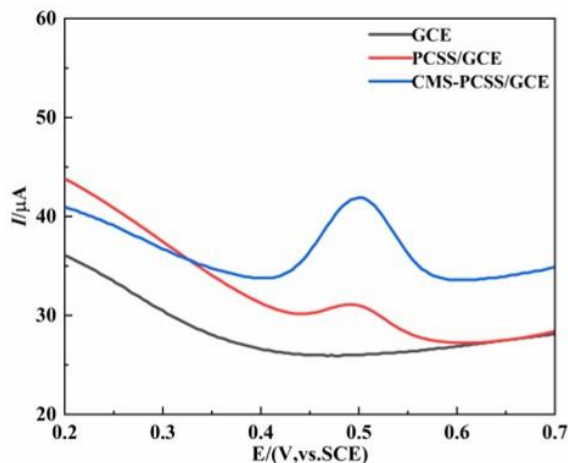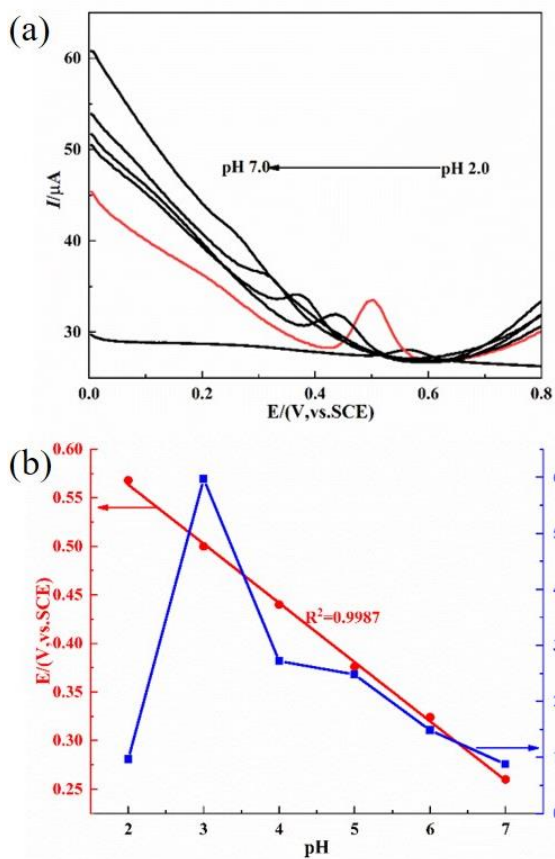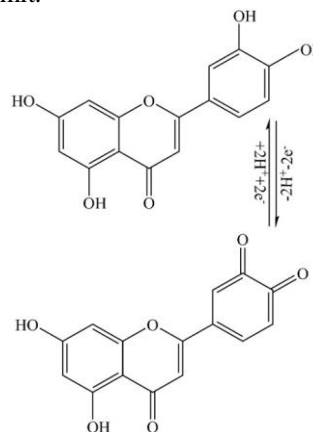

Fig. 8:   DPV of 10.0 µmol/L luteolin on CMS-PCSS/GCE in PBS with different pHs (a) and the relationships of E and I with pH (b).

As noted from Fig. 9(a), the effects of different scan rates on the CV response of 10.0 µmol/L luteolin were investigated in the PBS

(pH=3.0) at CMS-PCSS/GCE. When the sweep speed was between 20~200 mV/s, the peak currents of luteolin increased linearly with the square root of scan rate (v) (Fig. 9(b)), and the equations were expressed as I_{pa} (μA) = (2.298 ± 0.082) $v^{1/2}$ (mV/s) - (6.537 ± 0.794) and I_{pc} (μA) = (-2.352 ± 0.070) $v^{1/2}$ (mV/s) + (6.367 ± 0.675). These results showed that the electrochemical reaction process of luteolin was mainly a diffusion-controlled process [27]. The possible redox mechanism of luteolin at CMS-PCSS/GCE was shown in Scheme 1.

Fig. 9:   CV of 10.0 μmol/L luteolin on CMS-PCSS/GCE at different scan rates (20, 40, 60, 80, 100, 150, 200 mV/s) in PBS 3.0 (a) and the linear relationship of peak currents and the scan rates (b).

Fig. 10(a) shows the DPV charts acquired with different luteolin concentrations. Under the first-rank reaction conditions, the peak current (I_{pa}) increased linearly with the concentration (C) of luteolin in the range of 0.05~10.0 μmol/L (Fig. 10(b)). At lower luteolin concentrations (0.05~0.5 μmol/L), the regression equation was I_{pa} (μA) = (6.895 ±0.278) C (μmol/L) + (0.107 ± 0.078); and at higher luteolin level (0.5~10.0 μmol/L), the regression equation was I_{pa} (μA) = (1.339 ±0.053) C (μmol/L) + (3.341 ±

0.300). The minimum detectability was calculated to be 0.019 μmol/L (S/N=3). Compared with other reports (Table 2), the electrochemical sensor of luteolin designed in this paper displayed a lower detection limit.

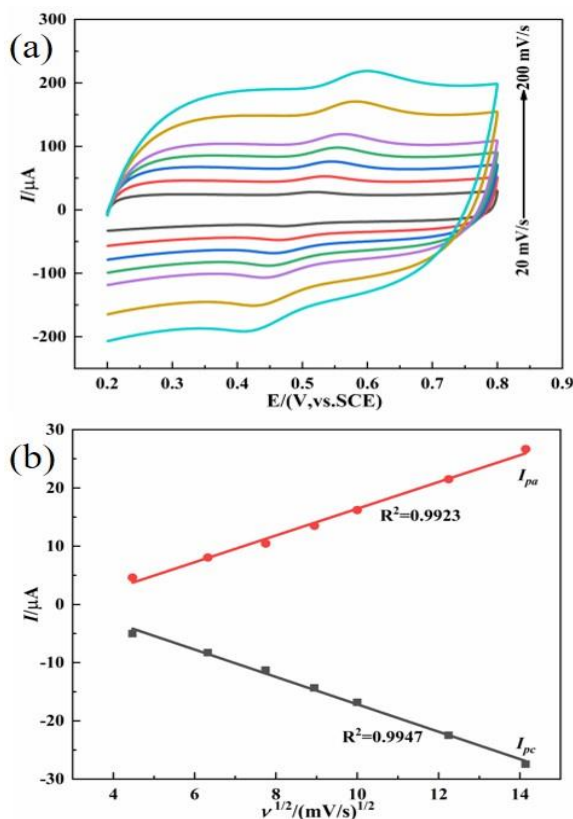Scheme-1:   Possible redox mechanism of luteolin at CMS-PCSS/GCE.
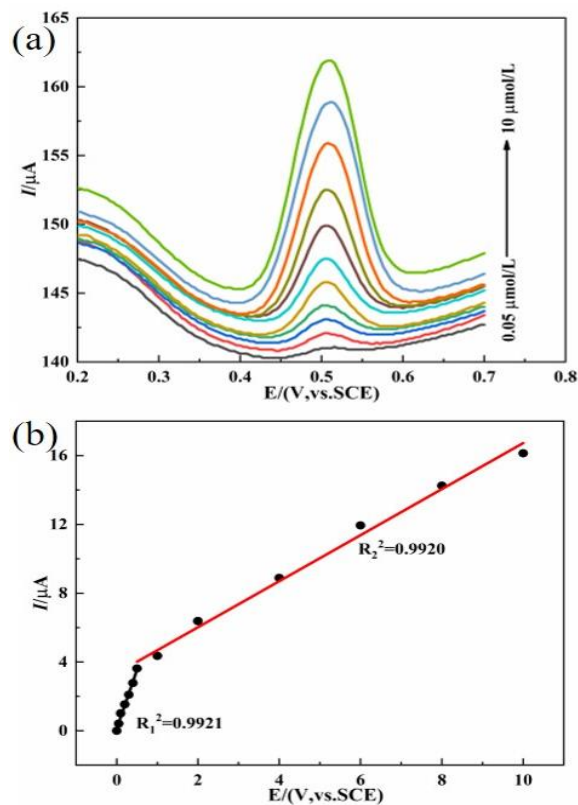

Fig. 10: DPV curves of luteolin with different concentrations (0.05, 0.1, 0.2, 0.3, 0.4, 0.5, 1.0, 2.0, 4.0, 6.0, 8.0, 10.0 μmol/L) in pH 3.0 PBS (a) and the relationship between I and luteolin concentration (b).

Table-2: Comparison of differentmethods for luteolin determination.

Electrode	Detection limit (µmol/L)	Reference
CDs–LTL	0.07	[12]
Nafion-AuNFs-BPC/GCE	0.07	[13]
PDDA-G-CNTs/β-CD/GCE	0.02	[4]
CMS-PCSS/GCE	0.019	This work

Anti-interference, reproducibility, and stability

The different potentially interfering compounds, which may exist in real samples of luteolin, were added to PBS (pH 3.0) containing 10.0 µmol/L luteolin to evaluate the possible analytical application of CMS-PCSS/GCE. The results showed that 50-fold KCl, NaNO$_3$, Fe$_2$(SO$_4$)$_3$, CaCl$_2$ and 10-fold glucose, uric acid, ascorbic acid, naringenin did not affect the response current value of luteolin more than 5%, it indicated that the sensor owned superior anti-interference ability.

The CMS-PCSS/GCEs were prepared in parallel for detecting 10.0 µmol/L luteolin in PBS (pH 3.0) in order to appraise the reproducibility of the sensor. The relative standard deviation (RSD) of the peak current from six electrodes was 4.8%, the RSD of one electrode for 10 times continuous detection under the same conditions was 3.6%. These results demonstrated that the CMS-PCSS/GCE has good reproducibility. After the CMS-PCSS/GCE was stored in the refrigerator at 4 °C for 14 days, the RSD of its initial current response value was 3.7%, which revealed the stability of the sensor was excellent.

Samples detection

To estimate the applicability of the CMS-PCSS/GCE, the Duyiwei capsule and healthy human urine samples were used. One capsule was dissolved in 5 mL ethanol and ultrasonic for 3 hours. The 5 mL extract was diluted to 10 mL with PBS (pH 3.0) to obtain the sample solution. The fresh urine sample of healthy people was centrifuged at 3000 rpm for 10 min to remove the excess protein in the urine sample, and then the supernatant was diluted to a uric acid content of 100 µmol/L, stand-by. The determination data was summarised in Table 3. The above results showed that the electrochemical method was accurate and suitable for analysing actual samples of luteolin.

Conclusion

In the paper, the waste sorghum straw was pyrolysed into biochar in the molten NaCl environment. Compared with PCSS, the CMS-PCSS prepared in the molten salt environment had a higher degree of graphitization, more developed specific surface area and pore structure, which endowed CMS-PCSS/GCE surface with lower electron transfer resistance and larger electroactive surface area, thus in the electrochemical sensing process, the CMS-PCSS/GCE showed a lower detection limit of luteolin, the detection range and limit was 0.05-10.0 µmol/L and 0.019 µmol/L, respectively. In addition, this sensor had good anti-interference ability, excellent repeatability and stability. In actual sample testing for the luteolin, the CMS-PCSS/GCE performed well. Besides, the preparation method of material was more in line with the idea of green chemistry.

Conflicts of interest

There are no conflicts to declare.

Acknowledgements

Table-3: Determination results of luteolin in different real samples (n=3).

Sample	Detected(µmol/L)	Added(µmol/L)	Total(µmol/L)	Recovery(%)	RSD(%)
Duyiwei capsule	2.32	1	3.34	100.6	3.35
		2	4.29	99.3	3.71
		4	6.30	99.7	3.75
Urine	-	2	2.01	100.5	4.02
		5	5.05	101.0	3.95
		10	9.96	99.6	4.13

References

1. H. Dong, X. C. Yang, J. P. He, S. Cai, K. J. Xiao, L. Zhu, Enhanced antioxidant activity, antibacterial activity and hypoglycemic effect of luteolin by complexation with manganese(II) and its inhibition kinetics on xanthine oxidase. *RSC Adv.* **2017**, *7*, 53385-53395.

2. J. Liu, H. Cheng, H. Xie, G. L. Luo, Y. Y. Niu, S. Y. Zhang, G. J. Li, W. Sun, Platinum nanoparticles decorating a biomass porous carbon nanocomposite-modified electrode for the electrocatalytic sensing of luteolin and application. *RSC Adv.* **2019**, *9*, 33607-33616.

3. C. M. Park, Y. S. Song, Luteolin and luteolin-7-O-glucoside protect against acute liver injury through regulation of inflammatory mediators and antioxidative enzymes in GalN/LPS-induced hepatitic ICR mice. *Nutr. Res. Pract.* **2019**, *13*, 473-479.

4. D. B. Lu, S. X. Lin, L. T. Wang, T. Li, C. M. Wang, Y. Zhang, Sensitive detection of luteolin based on poly(diallyldimethylammonium chloride)-functionalized graphene-carbon nanotubes hybrid/β-cyclodextrin composite film. *J. Solid State Electrochem.* **2014**, *18*, 269-278.

5. T. N. Wu, C. Z. Yu, R. Li, Determination of flavonoids in Flos Chrysanthemi and Flos Chrysanthemi Indici by capillary electrophoresis. *Instrum. Sci. Technol.* **2017**, *45*, 412-422.

6. S. Sagi, B. Avula, Y. H. Wang, J. P. Zhao, I. A. Khan, Quantitative determination of seven chemical constituents and chemo-type differentiation of chamomiles using high-performance thin-layer chromatography. *J. Sep. Sci.* **2014**, *37*, 2797-2804.

7. A. O. Silva, A. D. Alves, D. A. Almeida, S. O. Balogun, R. G. Oliveira, A. A. Aguiar, I. M. Soares, P. G. Marson-Ascencio, S. D. Ascencio, D. T. Martins, Evaluation of anti-inflammatory and mechanism of action of extract of Macrosiphonia longiflora (Desf.) Müll. *J. Ethnopharmacol.* **2014**, *154*, 319.

8. J. Meirinhos, B. M. Silva, P. Valentao, R. M. Seabra, J. A. Pereira, A. Dias, P. B. Andrade, F. Ferreres, Analysis and quantification of flavonoidic compounds from Portuguese olive (Olea Europaea L.) leaf cultivars. *Nat. Prod. Res.* **2005**, *19*, 189-195.

9. G. Maduraiveeran, M. Sasidharan, V. Ganesan, Electrochemical sensor and biosensor platforms based on advanced nanomaterials for biological and biomedical applications. *Biosens. Bioelectron.* **2018**, *103*, 113-129.

10. L. T. Zhu, X. D. Wang, Y. X. Han, Y. M. Cai, J. H. Jin, H. M. Wang, L. P. Xu, R. J. Wu, A PVC/polypyrrole sensor designed for beef taste detection using electrochemical methods and sensory evaluation. *Meat Sci.* **2018**, *137*, 1-8.

11. T. W. Chen, R. Ramachandran, S. M. Chen, G. Anushya, K. Ramachandran, Graphene and Perovskite-Based Nanocomposite for Both Electrochemical and Gas Sensor Applications: An Overview. *Sensors.* **2020**, *20*, 6755.

12. Q. Q. Sun, Y. W. Long, S. Pan, H. Liu, J. L. Yang, X. L. Hu, Carbon dot-based fluorescent probes for sensitive and selective detection of luteolin through the inner filter effect. *Luminescence.* **2018**, *33*, 1401-1407.

13. X. L. Niu, Y. Huang, W. L. Zhang, L. J. Yan, L. K. Wang, Z. F. Li, W Sun, Synthesis of gold nanoflakes decorated biomass-derived porous carbon and its application in electrochemical luteolin sensing. *J. Electroanal. Chem.* **2021**, *880*, 114832.

14. S. Vaithilingam, T. M. Ramanujam, Development of rice straw black liquor based porous carbon-poly(aniline-co-methoxy aniline) as supporting for electrochemical performances of alcohol oxidations. *Ionics.* **2018**, *24*, 3923-3935.

15. H. G. Wang, F. F. Wen, Y. J. Chen, T. Sun, Y. Meng, Y Zhang, Electrocatalytic determination of nitrite based on straw cellulose/molybdenum sulfide nanocomposite. *Biosens. Bioelectron.* **2016**, *85*, 692-697.

16. W. X. Kong, F. Zhao, H. J. Guan, Y. F. Zhao, H. S. Zhang, B. Zhang, Highly adsorptive mesoporous carbon from biomass using molten-salt route. *J. Mater Sci.* **2016**, *51*, 6793-6800.

17. L. Yang, J. Qiu, Y. Wang, S. Guo, Y. Feng, D. Dong, J. Yao, Molten salt synthesis of hierarchical porous carbon from wood sawdust for supercapacitors. *J. Electroanal. Chem.* **2020**, *856*, 113673.

18. A. R. Kamali, J. G. Yang, Effect of molten salts on the structure, morphology and electrical conductivity of PET-derived carbon nanostructures. *Polym. Degrad. Stab.* **2020**, *177*, 109184.

19. A. R. Kamali, J. G. Yang, Q. Sun, Molten salt conversion of polyethylene terephthalate waste into graphene nanostructures with high surface area and ultra-high electrical conductivity. *Appl. Surf. Sci.* **2019**, *476*, 539-551.

20. G. L. Gao, L. Z. Cheong, D. Y. Wang, C, Shen, Pyrolytic carbon derived from spent coffee grounds as anode for sodium-ion batteries. *Carbon Resour. Convers.* **2018**, *1*, 104-108.

21. X. Ma, M. Cao, C. Hu, Bifunctional HNO_3 catalytic synthesis of N-doped porous carbons for CO_2 capture. *J. Mater. Chem. A* **2013**, *1*, 913-918.

22. X. Q. Chang, L. Zhou, X. W. Ou, C. S. Lee, J. W. Zhou, Y. B. Tang, Ultrahigh nitrogen doping of carbon nanosheets for high capacity and long cycling potassium ion storage. *Adv. Energy Mater.* **2019**, *9*, 1902672.

23. Y. Qian, S. Jiang, Y. Li, Z. Yi, J. Zhou, T. Q. Li, Y. Han, Y. S. Wang, J. Tian, N. Lin, Y. T. Qian, In situ revealing the electroactivity of P-O and P-C bonds in hard carbon for high-capacity and long-life Li/K-ion batteries. *Adv. Energy Mater.* **2019**, *9,* 1901676.

24. J. Chmiola, C. Largeot, P. L. Taberna, P. Simon, Y. Gogotsi, Desolvation of Ions in Subnanometer Pores and Its Effect on Capacitance and Double-Layer Theory. *Angew. Chem.* **2008**, *47*, 3392-3395.

25. D. S. Su, R. Schlcgl, Nanostructured Carbon and Carbon Nanocomposites for Electrochemical Energy Storage Applications. *ChemSusChem.* **2010**, *3*, 136-168.

26. X. D. Hou, W. Wu, F. Y. Zhao, W. C. Xie, Q. L. Yang, Construction of an electrochemical sensor with graphene aerogel doped with ZrO2 nanoparticles and chitosan for the selective detection of luteolin. *Microchim. Acta.* **2021**, *188*, 86.

27. Y. Z. Zhang, R. X. Sun, B. M. Luo, L. J. Wang, Boron-doped graphene as high-performance electrocatalyst for the simultaneously electrochemical determination of hydroquinone and catechol. *Electrochim. Acta.* **2015**, *156*, 228-234.